Electronic Supplementary Material (ESI) for RSC Advances.
This journal is © The Royal Society of Chemistry 2017

Supplementary Information

Steering Photoinduced Charge Kinetics *via* Anionic Group Doping in Bi_2MoO_6 for Efficient Photocatalytic Removal of Water Organic Pollutants

Yongxing Xing, Jing Zhang, Zhiliang Liu and Chunfang Du*

College of Chemistry and Chemical Engineering, Inner Mongolia University, Hohhot,Inner Mongolia, 010021, P. R. China.

E-mail: cedchf@imu.edu.cn; Fax: +86-471-4994375; Tel: +86-471-4994375

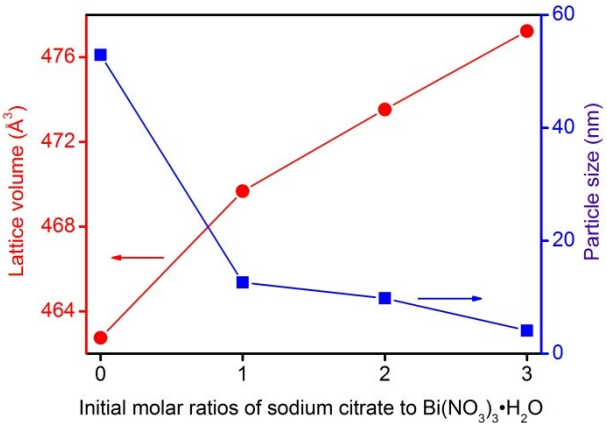

Fig. S1. Lattice volume and particle size as a function of initial molar ratios of sodium citrate to $Bi(NO_3)_3 \bullet H_2O$

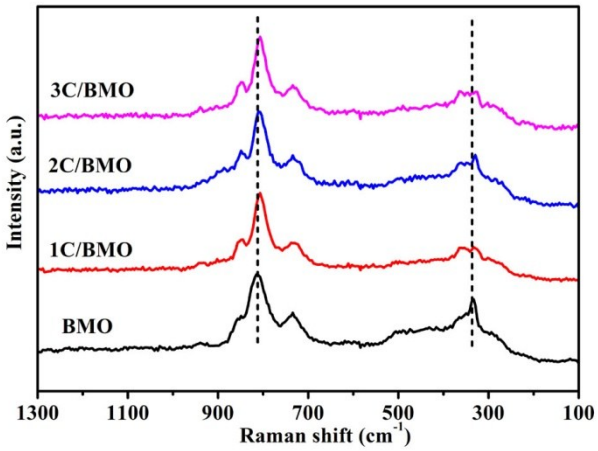

Fig.S2 Raman spectra of pristine BMO with different carbonate doping contents

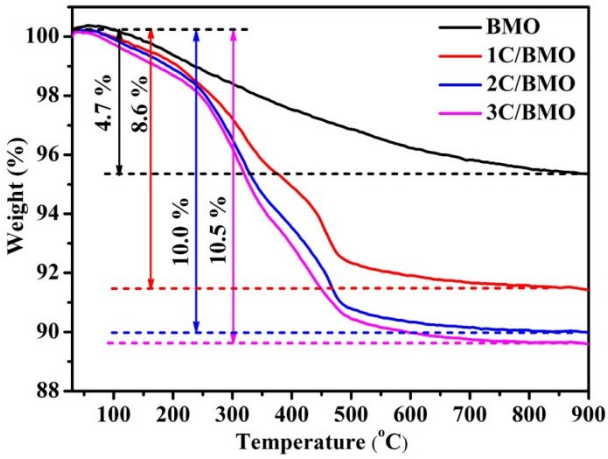

Fig. S3 TG curves of pristine BMO with different carbonate doping contents

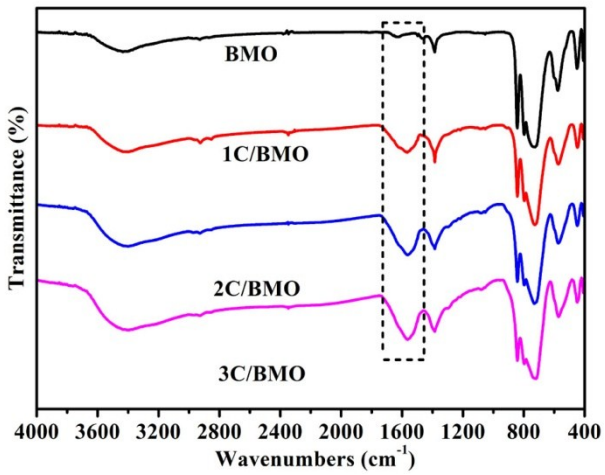

Fig. S4 FT-IR spectra of pristine BMO with different carbonate doping contents

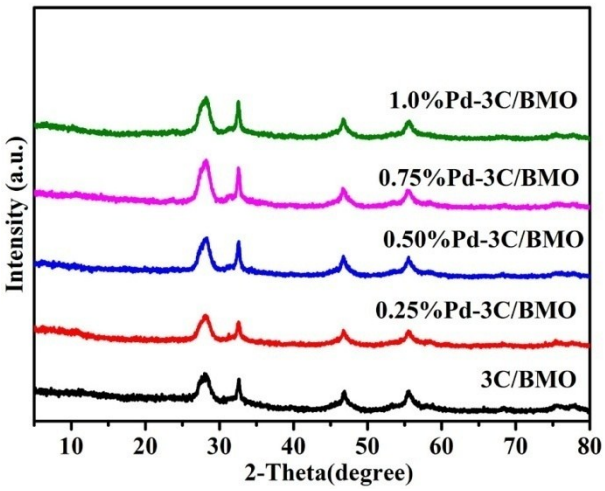

Fig. S5 XRS patterns of 3C/BMO with different Pd loading contents

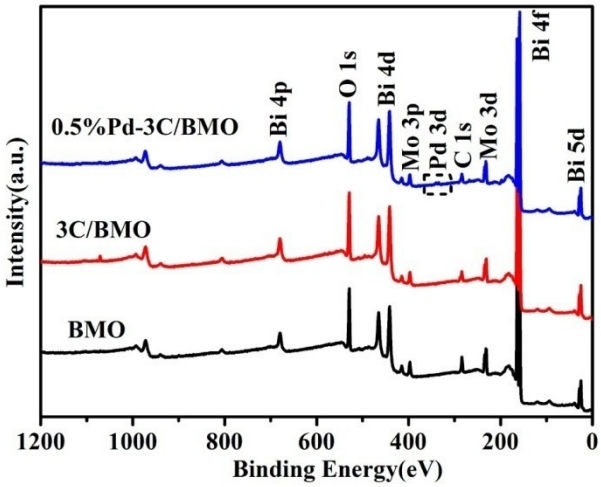

Fig. S6 The survey XPS spectra of pristine BMO, 3C/BMO and 0.5 % Pd-3C/BMO.

Table S1 Elemental composition determined by XPS data.

Sample	Bi/at %	O/at %	Mo/at %	C/at %[a]	Ag/at %	Au/at %	Pd/at %
BMO	14.807	47.186	6.872	0	-	-	-
3C/BMO	15.686	52.72	5.819	6.695	-	-	-
0.9%Ag-3C/BMO	16.34	50.493	6.007	6.812	1.038	-	-
1.2%Au-3C/BMO	14.617	51.419	5.432	7.004	-	0.063	-
0.5%Pd-3C/BMO	17.409	50.806	5.224	6.832	-	-	0.285

[a] The carbonate doping content was determined by eliminating the carbon reference C 1s signal at 284.8 eV.

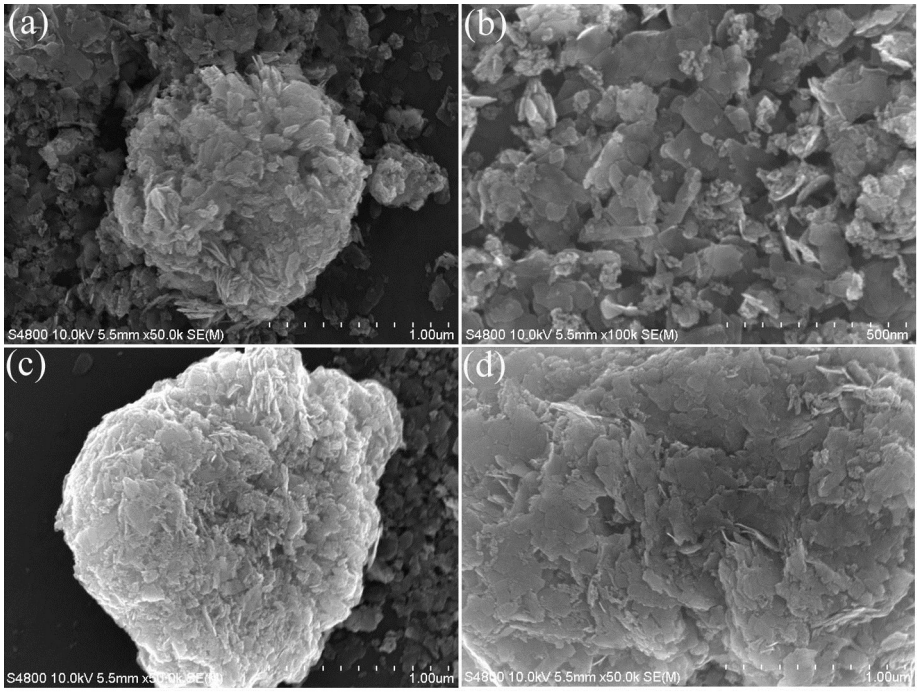

Fig.S7 SEM images of 1.2 % Au-3C/BMO (a, b) and 0.9 % Ag-3C/BMO (c, d).

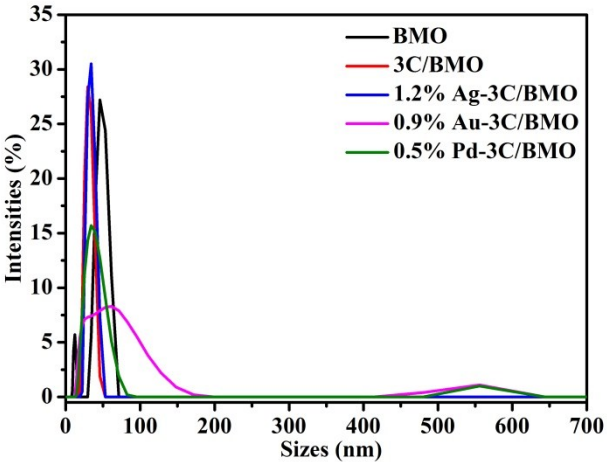

Fig. S8 Particle size distribution determined by zeta potential measurement.

The particle size distributions of various samples are conducted in Zeta sizer Nano ZS90.

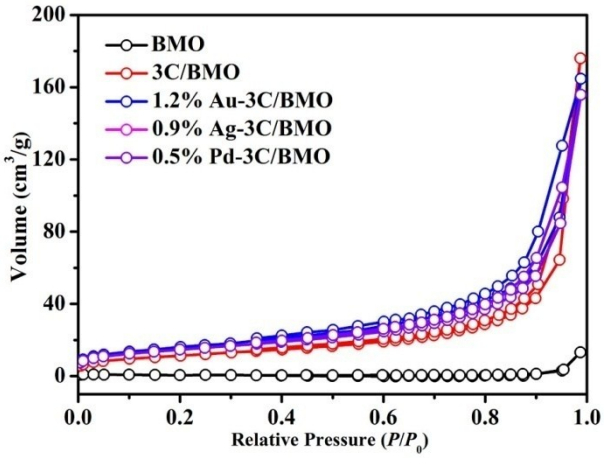

Fig. S9 N_2 adsorption-desorption isotherms of various samples

Table S2 Porous parameters of various samples

Samples	Specific surface area (m^2/g)	Pore volume (cm^3/g)
BMO	1.8	0.02
3C/BMO	40.8	0.27
1.2 % Au-3C/BMO	57.0	0.25
0.9 % Ag-3C/BMO	52.3	0.24
0.5 % Pd-3C/BMO	55.6	0.28

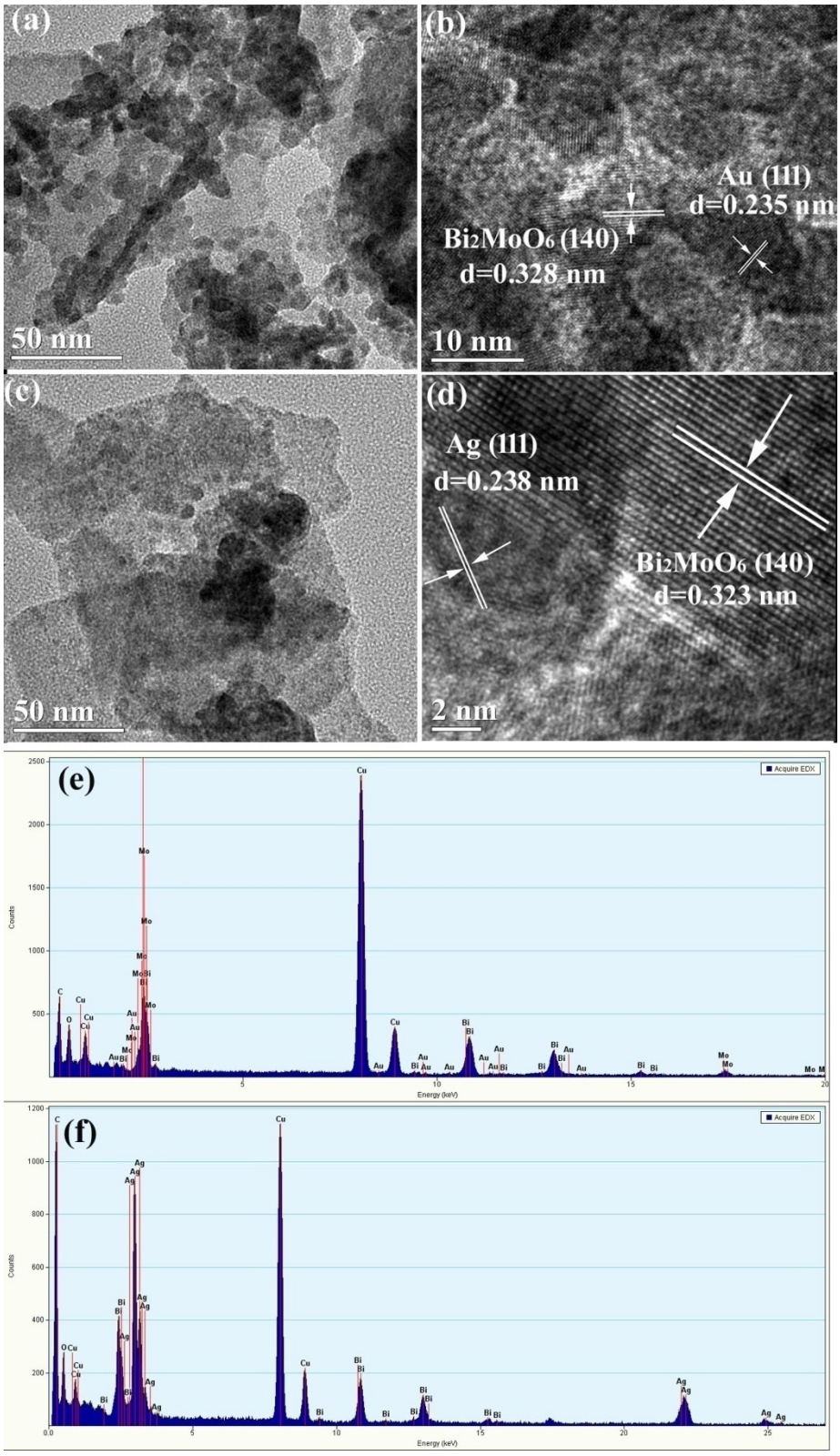

Fig. S10 TEM, HRTEM images and EDS spectra of 1.2 % Au-3C/BMO (a, b, e) and 0.9 % Ag-3C/BMO (c, d, f)

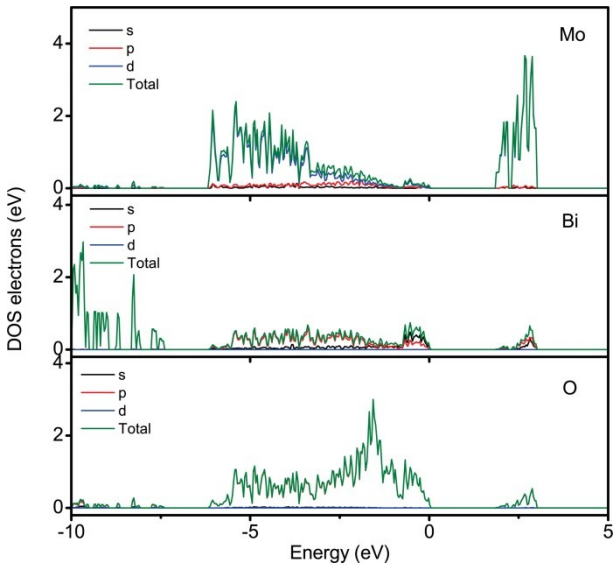

Fig. S11 Density of states for Mo, Bi, and O in Bi_2MO_6 model.

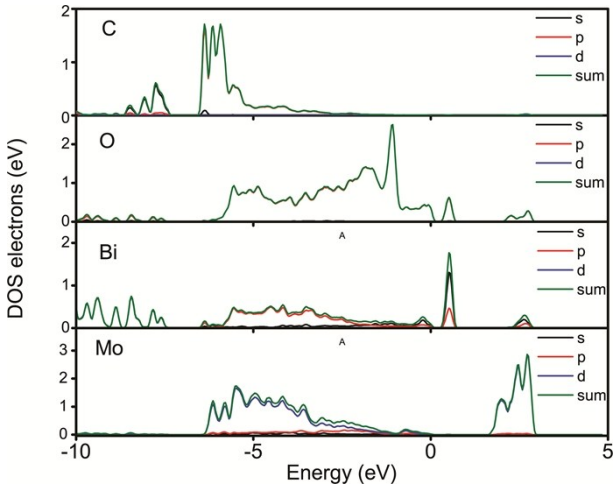

Fig. S12 Density of states for C, Mo, Bi, and O in CO_3^{2-} doped Bi_2MoO_6 model.

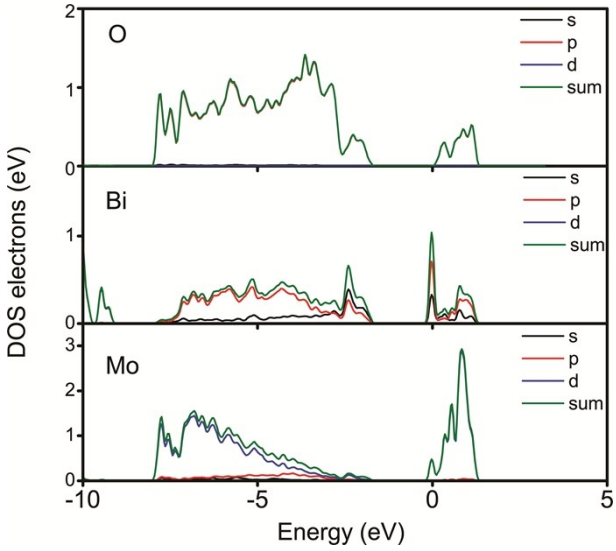

Fig. S13 Density of states for Mo, Bi, and O in Bi_2MoO_6 with oxygen vacancy model.

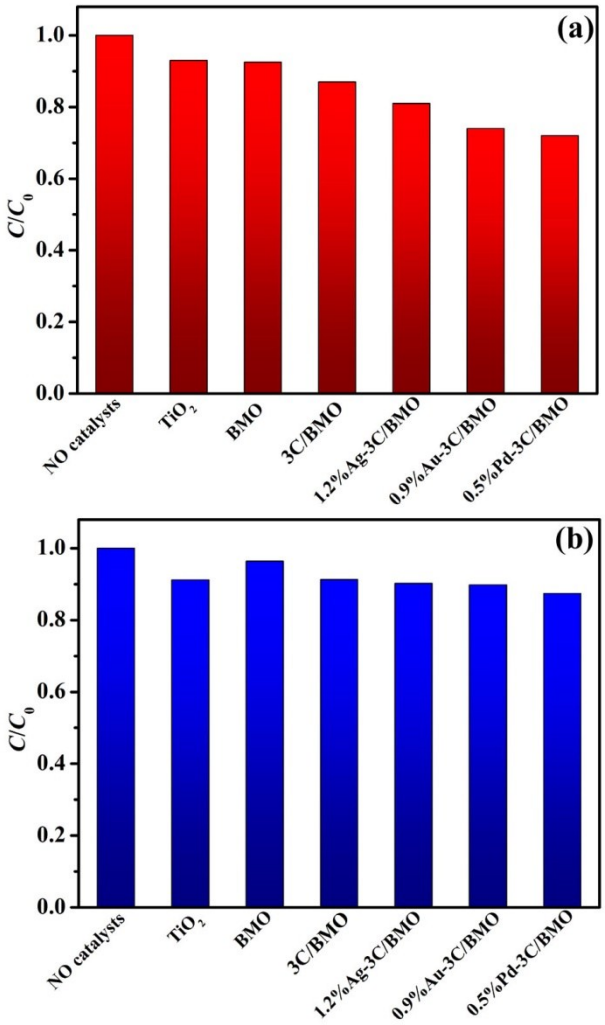

Fig. S14 Adsorption-desorption equilibrium experiments for RhB (a) and OPP (b) over various photocatalysts.

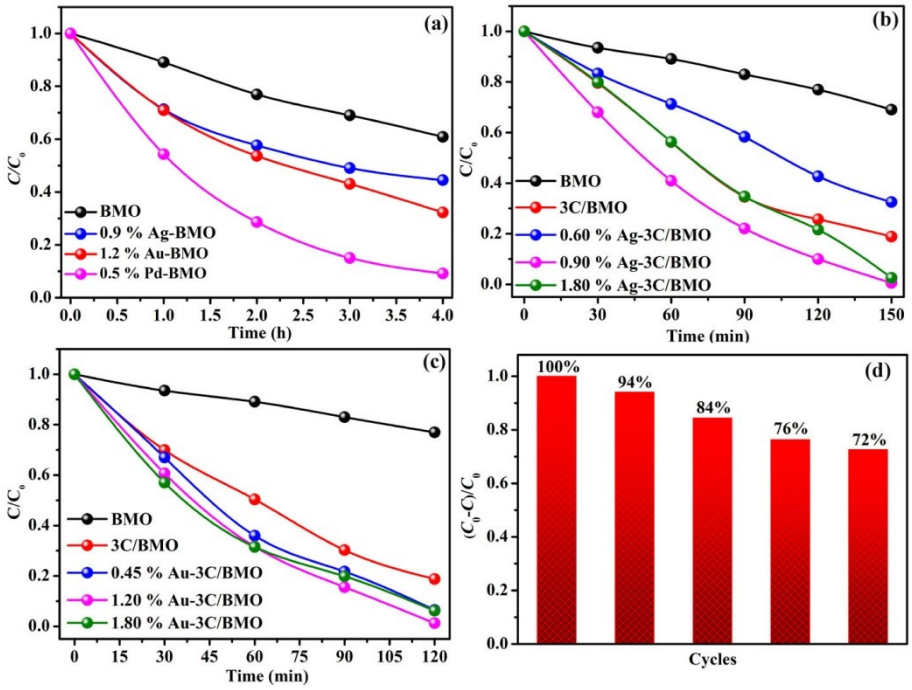

Fig. S15 The photocatalytic activities of pristine BMO with loaded various noble metals (a), pristine BMO and 3C/BMO with different Ag (b) and Au (c) loading contents with luminous powder of 300 W, cycle experiment of 0.5 % Pd-3C/BMO (d) with luminous powder of 500 W toward RhB under UV + visible light irradiation

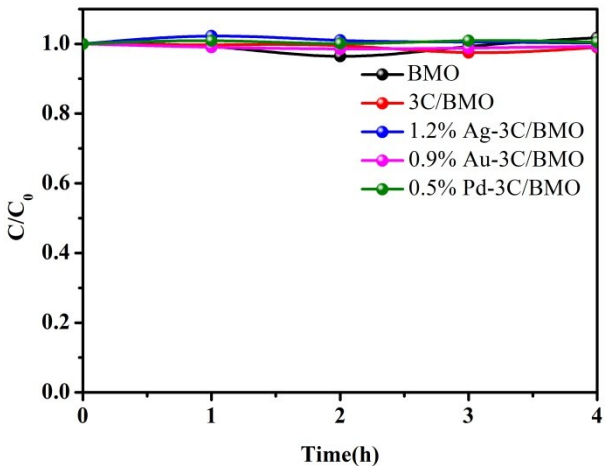

Fig. S16 The photocatalytic activities of pristine BMO, 3C/BMO as well as various noble metals loaded samples toward OPP degradation by using a bandpass filter (550 nm) with luminous power of 500 W.

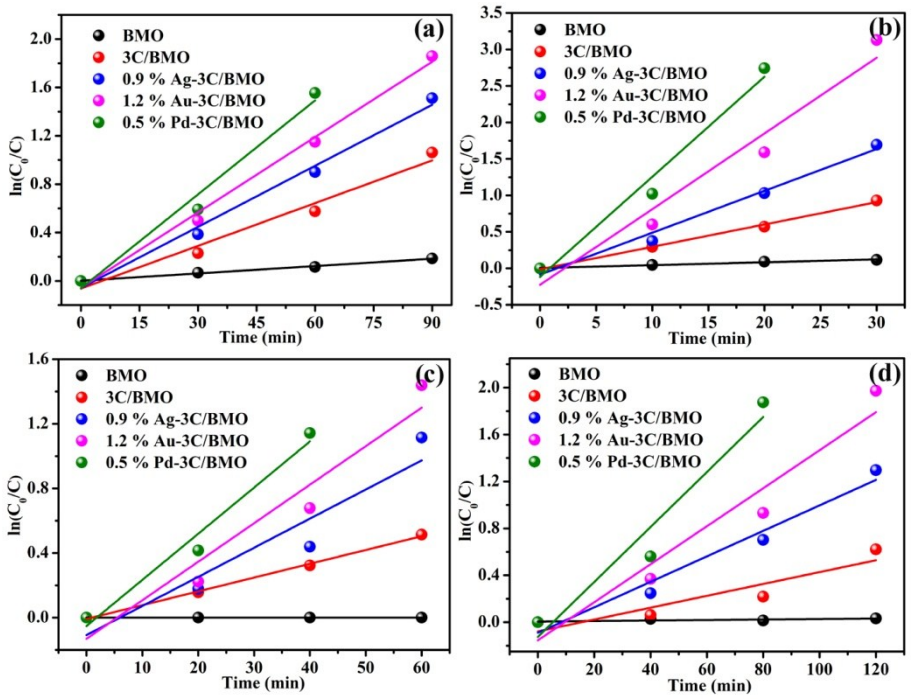

Fig. S17 Kinetic linear simulation curves of RhBphotodegradation under UV + visible light irradiation with luminous power of 300 W (a) and 500 W (b). Kinetic linear simulation curves of OPP photodegradation under UV + visible light irradiation (c) and visible light irradiation (d) with luminous power of 500 W over various samples.

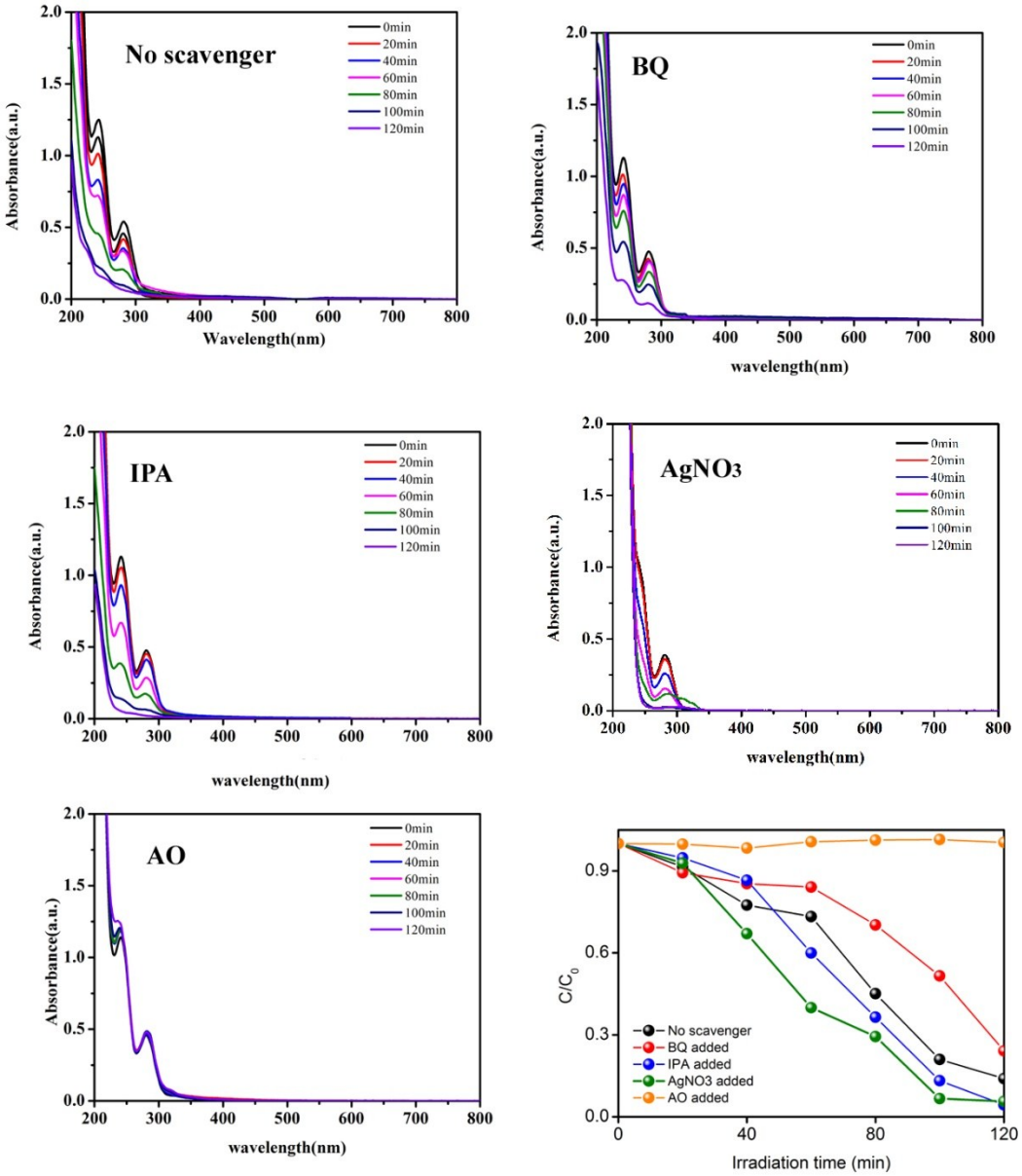

Fig. S18. UV-vis absorption spectra recorded during the photocatalytic degradation of OPP over 0.5 % Pd-3C/BMO by adding various scavenger species and the relation between C/C_0 and t.

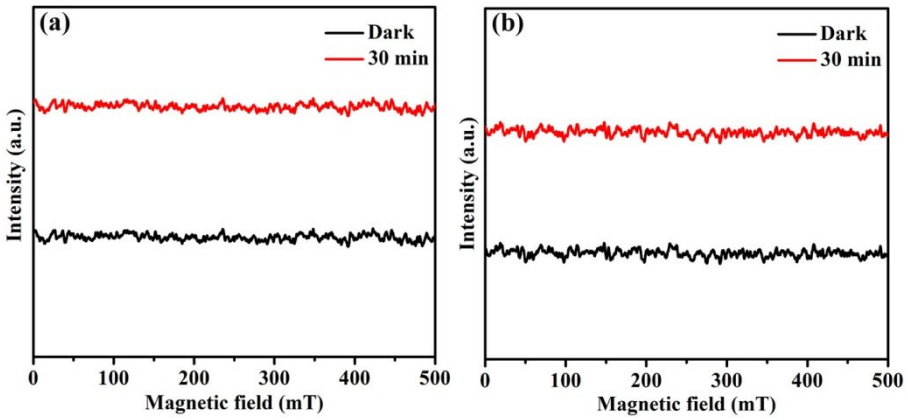

Fig. S19 ESR spectra of DMPO-·OH (a) and DMPO-·O_2^- adducts without photocatalysts in darkness and under visible light irradiation for 30 min